Components of the Plasma Membrane of Growing Axons. I. Size and Distribution of Intramembrane Particles

ROCHELLE K. SMALL and KARL H. PFENNINGER
Department of Anatomy and Cell Biology, College of Physicians and Surgeons, Columbia University, New York 10032. Dr. Small's present address is Department of Pathology (Immunology), Yale University, School of Medicine, New Haven, Connecticut 06510.

ABSTRACT The plasmalemma of mature and growing olfactory axons of the bullfrog has been studied by freeze-fracture. Intramembrane particles (IMPs) of mature olfactory axons are found to be uniformly distributed along the shaft. However, during growth, a decreasing gradient of IMP density is evident along the somatofugal axis. The size histograms of axolemmal IMPs from different segments of growing nerve reveal regional differences in the particle composition. The distribution of each individual size class of particles along the growing nerve forms a decreasing gradient in the somatofugal direction; the slope of these gradients varies directly with particle diameter. These size-dependent density gradients are consistent with a process of lateral diffusion of membrane components that are inserted proximally into the plasma membrane. The membrane composition of the growth cone, however, appears to be independent of these diffusion gradients; it displays a mosaic pattern of discrete domains of high and low particle densities. The relative IMP profiles of these growth cone regions are similar to one another but contain higher densities of large IMPs than the neighboring axonal shaft. The shifting distributions of intramembrane particles that characterize the sprouting neuron give new insights into cellular processes that may underlie the establishment of the functional polarity of the neuron and into the dynamics of axolemmal maturation.

The study of mechanisms involved in growth and assembly of the plasma membrane requires a cell preparation showing rapid expansion or turnover of total surface area or, preferably, of a discrete membrane region (e.g., 1, 22, 23). In most cells, however, it is difficult to identify and segregate distinct regions of the plasma membrane for analysis. The neuron is a notable exception: even before maturity, during neurite formation, its extreme polarity presents an ideal situation for isolating and comparing identified segments of its plasma membrane. An analysis of the spatial distribution of membrane components of growing neurons is likely to further our understanding of mechanisms used to expand the plasmalemma and to establish cell polarity (cf., 30–32).

Neurons grown in culture exhibit distinguishing properties of the plasmalemma at opposite ends of the neurite, i.e., in the perikaryon as compared to the distal neurite. This has been revealed by lectin binding studies (31), freeze-fracture analyses of intramembrane particles (7, 29), and electrophysiological studies (12, 17, 21, 37, 42).

In the present paper, we have begun a segmental analysis of neuronal plasmalemma using as a simple model system olfactory axons growing in vivo. The mature olfactory nerve, arising from receptor perikarya in the olfactory epithelium, consists of a homogeneous population of several million fine, unmyelinated axons that terminate in the olfactory bulb. When olfactory axons are severed, the residual portions of existing neurons completely degenerate, and neurons are formed *de novo* from epithelial stem cells (10). This provides well synchronized and uniform primary neuritic outgrowth (unlike regenerating axons, which sprout from the cut stumps).

Freeze-fracture analysis of the plasmalemma along the growing axon permits a quantitative survey of putative integral membrane proteins or their clusters on the basis of size. Regional differences in membrane protein content are expected to be reflected, at least to some degree, in the total density and the size histogram of intramembrane particles (IMPs)[1] in specific nerve segments (cf. Discussion). Indeed, in cultured explants, the plasma membrane of the axon's grow-

[1] *Abbreviations used in this paper:* IMP, intramembrane particle; E, external; P, protoplasmic leaflet.

THE JOURNAL OF CELL BIOLOGY · VOLUME 98 April 1984 1422–1433

ing tip has far fewer IMPs than that of the more proximal axonal shaft (29). The present paper extends this observation to an in vivo preparation. Most importantly, it describes the density gradients and size distributions of IMPs along the shaft of growing neurons and compares these data with those obtained from mature neurons. The companion papers provide a mathematical analysis and a dynamic model of IMP distribution (36) and present the results of saxitoxin-binding studies comparing mature and growing olfactory nerves (38).

MATERIALS AND METHODS

Animals: Large adult bullfrogs (*Rana catesbeiana*) of at least 400 g weight were obtained from West Jersey Biological Supply (Wenonah, NJ) and maintained in the laboratory for 1 mo before treatment. They were kept at ambient room temperature (20–23°C) and housed in a system that automatically flushed fresh water through their cage four times a day. The frogs were force fed a mixture of pureed chicken and cod liver oil once a week.

Surgery: As shown schematically in Fig. 1, axons arising from bipolar receptor neurons located in the nasal epithelium travel through the nasal submucosa before converging on each side into a single nerve of ~1 mm diameter. The nerve then runs in a bony canal for an average distance of 0.9 cm before entering the olfactory bulb where the axons terminate in glomeruli. Since olfactory perikarya are spread out in the large cup-shaped olfactory epithelium, the length of the intranasal portion of the axon varies depending on perikaryal location. Therefore, the midpoint of the nasal epithelium was selected as the average origin for measuring axonal length. In the olfactory epithelium of the adult bullfrog, receptor cells normally turn over slowly (9). Surgical lesion of the olfactory nerve leads to rapid retrograde degeneration of the residual portion of axons and their neuronal perikarya (10). Subsequently, mitosis occurs among epithelial stem cells, and new receptors differentiate and extend neurites that grow towards the olfactory bulb within the next weeks.

For these studies, we removed olfactory nerves bilaterally from 15 adult bullfrogs in order to induce formation of growing nerves for subsequent study. Animals were anesthetized with ~3 ml of 3% (wt/vol) ethyl-m-aminobenzoate (MS-222) injected into the ventral lymph sac. To remove the mature nerve, we first incised the skin along the midline reaching from the level of the nares to the center between the eyes. The resulting skin flaps were moved to either side, and a rectangular opening was drilled into the skull and the underlying cartilage to expose the canal in which the nerves travel. The epineurium was opened longitudinally, and the exposed segment was cut and removed from both nerves. Care was taken to avoid transecting the epineurial sheath and accompanying blood vessels. After closing the wounds by replacing the cartilage plate and suturing the skin, we allowed bullfrogs to survive for a period of 5 wk.

The technique of removing most of the existing nerve was selected because it consistently produced well-synchronized neuritic outgrowth that contained only minimal amounts of debris from degenerating cells, white blood cells, or scar tissue. Furthermore, it avoided contamination of our samples with long-term surviving severed axons (cf. 5).

Microscopy: For thin sectioning, we fixed olfactory nerves from both intact controls and operated animals by perfusion of the anesthetized frogs with 1.5% glutaraldehyde, followed by 4% glutaraldehyde in 0.1 M phosphate buffer (pH 7.3) with 0.32 mM $CaCl_2$ and 0.12 M glucose. The fixative was introduced retrogradely into the dorsal aorta and simultaneously dripped directly into the nasal cavity. The olfactory nerves and mucosa were then dissected out, immersed in 4% glutaraldehyde for 1 h and washed in 0.2 M arsenate buffer, first with 2 mM $CaCl_2$, then with 5 mM $CaCl_2$ added to improve membrane preservation. The nerves were then dissected free of their epineurial sheath and divided into a series of segments along the somatofugal axis. (The term "proximal" here designates axonal segments near the peripherally located perikarya, while "distal" refers to segments closer to the olfactory bulb, rather than the animal's periphery.) Tissues were postfixed in 2% OsO_4 in 0.2 M arsenate buffer with 10 mM $CaCl_2$ for 40 min and then washed overnight in 0.17 M NaCl. After block staining with 0.5% uranyl magnesium acetate in saline, specimens were dehydrated with ethanol, transferred to propylene oxide, and embedded in Epon 812. Thin sections were counterstained with uranyl acetate and lead citrate. All chemicals were reagent grade. Uranyl magnesium acetate was obtained from Electron Microscopy Sciences (Ft. Washington, PA).

For freeze-fracture, aldehyde-fixed tissue was washed in 0.1 M phosphate buffer to which 25% glycerol was slowly added. Tissue was finally left in 25% glycerol for 30 min and then divided into a series of identified proximodistal segments beginning with the perikarya in the epithelium. Nerve segments were transferred to gold alloy specimen holders, frozen by immersion in Freon 22, and then stored in liquid nitrogen. Nerves were fractured in a Balzers BAF 300 (Balzers Corp., Nashua, NH), at −115°C and a vacuum of $<10^{-6}$ mbar, and were "etched" for 20 s. The platinum-carbon films, 2 nm thick and applied at a 45° angle, were produced with an electron beam gun in conjunction with a quartz crystal thin film monitor. A drop of 0.5% collodion in amyl acetate was placed on the replicated tissue still held in the carrier. Replicas were floated off in a gradually increased concentration of Clorox (The Clorox Co., Oakland, CA) in distilled H_2O. After tissue digestion was complete, replicas were washed in distilled H_2O and picked up on 75-mesh Formvar-coated grids. Grids were briefly washed in amyl acetate to remove collodion films and then examined in a JEOL JEM 100C electron microscope calibrated with a replica grating (E. F. Fullam, Schenectady, NY).

Analysis of Replicas: Fractured areas that exposed large expanses of the protoplasmic (P) and external (E) faces of the axolemma were randomly photographed at × 26,000. Electron micrographs were printed at a final magnification of × 67,600 and coded for blind analysis. The entire analysis was carried out twice by the same investigator, on different electron micrographs, and the results were consistent. Blind comparison measurements by a second investigator yielded very similar data, to within 10%. For IMP density measurements, all exposed P-faces of longitudinally fractured axons contained in a micrograph were included in the sample. To avoid distortion from axolemmal curvature, we restricted density estimates to a longitudinal strip about one half of the axon diameter in width, midway from either edge of the axon. This slight curvature would be expected to produce systematically a 9% overestimate in our particle densities. The measurement of narrow axolemmal areas meant that large numbers of individual axons had to be sampled, most contributing $<0.1\ \mu m^2$ of measurable area. However, the combined axonal P-face samples from each replica averaged $6.9\ \mu m^2$. Smaller numbers of axonal E-faces were also sampled from each micrograph. Axonal growth cones were recognized in replicas as irregularly shaped, filopodia-bearing enlargements at the tip of a long, slender process (39). Axonal growth cones are not as easily recognized in vivo as the flattened, palm-shaped structures seen in tissue culture (4, 43). The number of axons, total surface area and number of replicas analyzed are shown in Table I. All these figures were included in the calculation of the overall IMP densities of each segment. For the generation of IMP size profiles, we selected from each nerve segment samples consisting of 10 to 20 axons, each of whose total IMP density was within one standard deviation of the average density of that segment. This helped to reduce the noise in the data, especially for the larger, sparser IMPs. Plasma membranes of Schwann cells were also examined.

The perikarya of olfactory neurons are located in a pseudostratified epithelium containing three cell types whose nuclei are loosely arranged in separate zones. The nuclei of olfactory neurons occupy a position intermediate to the more apical supporting cell nuclei and the basally located stem cells (Fig. 1). In replicas, perikaryal plasma membranes of olfactory neurons were identified on the basis of position, restricting the samples to cells whose nuclei were in the lower third quarter of the epithelium, and, secondly, cytological features, such as size and shape of the perikarya and their apical and basal processes, paucity of cytoplasm surrounding the nucleus, and the absence of secretory granules. Large, flat expanses ($>0.5\ \mu m^2$) of perikaryal plasma membrane were exposed in fractures through the epithelium.

IMP size histograms were calculated by measuring the diameter of the particles along an axis perpendicular to the direction of shadowing. Electron

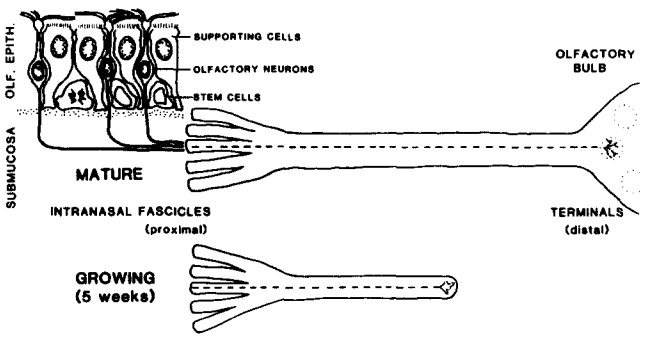

FIGURE 1 Schematic of the bullfrog olfactory system. Axons in the mature nerve arise from primary sensory neurons located in the olfactory epithelium. Axons travel in fascicles through the submucosa before converging to a single nerve of ~1 mm diameter. Olfactory neurons are continuously replaced throughout life; turnover can be synchronized by lesioning the mature nerve. The resulting mitoses of stem cells lead to the differentiation of new neurons whose neurites have been examined during growth in this paper.

micrographs were viewed under a zoom dissecting microscope and enlarged to a final magnification of approximately × 650,000, dependent upon grain of the replica. IMP diameters were measured with a 0.1-mm ruler placed directly on the micrograph. Particles that deviated strongly from a spherical configuration were assigned to a special IMP class designated "oblong;" oblongs usually consisted of either a string of extremely small, almost confluent beads, or a narrow elongated profile (see, e.g., arrowhead in Fig. 5*A*). In order to compare axolemma from corresponding regions of nerves that had grown for differing

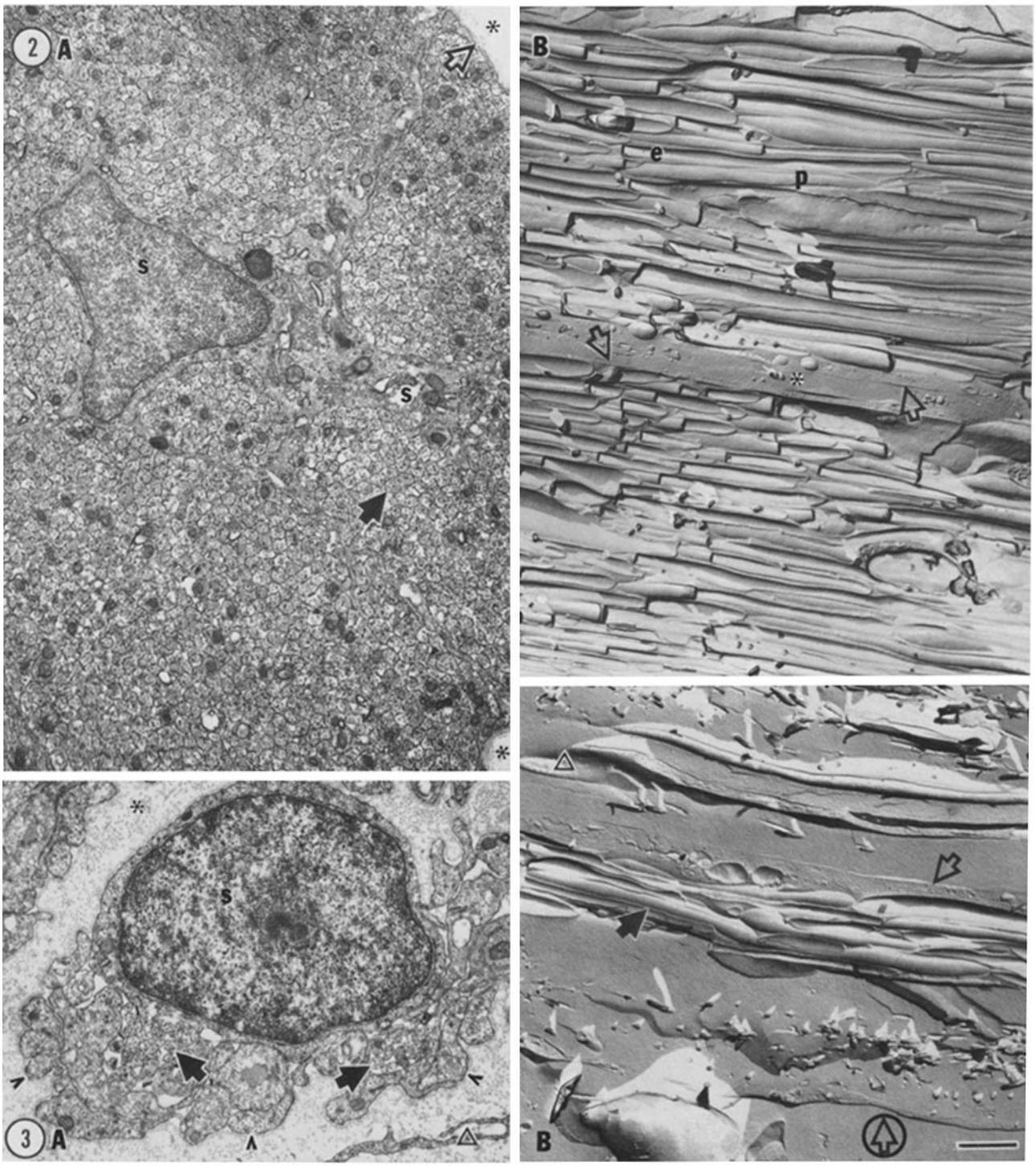

FIGURES 2 and 3 Mature bullfrog olfactory nerve; middle segment. (*A*) Cross-section of a small portion of one of the many fascicles that form the mature olfactory nerve. Olfactory axons (solid arrow) of highly uniform size are tightly packed into compartments formed by Schwann cell (*s*) processes. A flattened Schwann cell layer (open arrow) envelops the fascicle. Asterisks indicate extracellular space with collagen fibers. (*B*) Longitudinal fracture through the mature olfactory nerve reveals large numbers of P-faces (*p*) and E-faces (*e*) of axons. Thin Schwann cell profiles (open arrows) separate axonal bundles from extracellular space (asterisk). × 11,000. Fig. 3: Growing olfactory nerve (5-wk-postoperative); midsegment. (*A*) In the growing nerve, small groups of axons (solid arrows) are engulfed by several rounded Schwann cell (s) processes (arrowheads). Thin processes of connective tissue cells (open triangle) partition the collagen-filled extracellular space (asterisk). (*B*) In freeze-fracture, small groups of growing axons (solid arrow) are enveloped by a broad Schwann cell process (open arrow). Open triangle indicates a supporting cell. Circled arrow indicates approximate shadowing direction. Bar, 1 μm. × 11,000.

distances, segment lengths and positions were expressed as percent values of total length of the nerve from which they were derived. These percentages were then reconverted to millimeters on the basis of the average lengths measured in mature and 5-wk-postoperative nerves.

The distribution patterns of IMPs along the somatofugal axis of growing axons were analyzed by curve fitting with various linear and nonlinear functions, using a Hewlett-Packard programmable calculator. Exponential functions were found to yield the best correlation coefficients. However, the densities of most IMP size classes approached an asymptote above zero. This suggested the presence of a base-line level of IMPs throughout the axolemma. When the densities of each IMP size class in the growth-cone-associated vesicles (see below) were used as the asymptotes (see c term in Table III and hatching in Fig. 10*A*) the correlation coefficients (r^2) improved to >0.90.

In the vesicles (~80 nm diameter) that characteristically occur in clusters in growing axons, IMP densities and sizes were assessed in the concave, or P-fracture face, using a modification of the procedure of Losa et al. (18). A circle was selected from a series of different test circles of known area and positioned over the center of the vesicle. The largest test circle fitting into the vesicle was selected with the restriction that one half of the area it enclosed was free of any cast shadow that might obscure IMPs. Particles within this half circle were counted and measured as described above. For those vesicles not showing a cast shadow, all particles within the entire test circle were included in the analysis.

Histograms of diameters of axon shafts were determined from micrographs (× 41,600) of randomly selected regions of cross-sectioned nerves, in both thin-sectioned and freeze-fractured material. In cases where axons were elliptical, both major and minor axes were measured, and the diameter of a circle of equivalent area was calculated ($d = \sqrt{d_1 d_2}$). No attempt was made to measure the diameter of growth cones because they are too irregular in shape.

The significance of differences was evaluated with the Student's t test, using two-tailed significance levels.

RESULTS

Histology of Mature and Growing Olfactory Nerves

Axons of the mature olfactory nerve of the bullfrog comprise a remarkably homogeneous population of small-diameter fibers as shown in Fig. 2 (as well as in the histogram in Fig. 4*A*). Axonal diameters average 0.15 ± 0.05 μm (±SD), a value that is smaller than those calculated for olfactory axons of pike (cf. 16, 41) or garfish (6). 95% of fiber diameters are in the range of 0.08 to 0.25 μm. Mean diameters obtained from thin-sectioned and freeze-fractured material were virtually identical. Axons with the largest diameters usually contain a mitochondrion, or, less frequently, a cluster of clear vesicles. No significant differences in axonal diameter or morphology are observed regionally along the mature nerve. As seen in Fig. 2*A*, a Schwann cell envelops a large bundle of olfactory axons with a flattened process which also ramifies within the bundle to form compartments (cf. 8). The unique morphology of the olfactory nerve results in an unusually high ratio of axolemma to Schwann cell plasmalemma (11; cf. our companion paper [38]).

By 5 wk after surgical removal of mature olfactory nerves, growing nerves already extend into the bone canal, traversing between 60 and 75% of the distance to their targets. The mean length of growing nerves 5 wk after surgery is 9.7 ± 0.5 mm (±SEM; cf. 38). This suggests an average growth rate of 0.35 mm/d if the initial week after surgery is assumed to be spent for degenerative processes and mitotic activities preceding neuritic outgrowth.

Thin sections through growing nerves show that the physical relationship of axons to Schwann cells is similar to that seen in mature nerves (Fig. 3*A*). However, far fewer axons are contained in each Schwann cell compartment, and the Schwann cell envelope consists of relatively thick profiles, rich in intermediate filaments and lipid droplets, rather than flattened processes. In regions containing small axon bundles, such as that shown in Fig. 3*A*, several Schwann cell profiles, often overlapping, may contribute to the envelope of one fiber bundle. Larger axon bundles are engulfed by a flattened Schwann cell process, resembling that seen in mature nerve. In growing nerve, axon fascicles are widely separated by collagen-filled extracellular space that is partitioned by thin processes of supporting cells. The relative amounts of axolemma in mature and growing nerves have been assessed by stereological methods, and these results are presented in one of our companion papers (38).

A comparison of axonal diameters in segments of the growing nerve 5 wk after surgery suggests significant tapering of the axon shafts in the somatofugal direction as well as an increase in the variability of the size of growing axons (Fig. 4*B*). The average diameter of round axonal profiles decreases from 0.15 ± 0.05 μm in the intranasal segments to 0.13 ± 0.07 μm in the most distal segment ($P < 0.001$). A particularly striking feature of the growing nerve is the occurrence of extremely small axonal processes (<0.10-μm diameter). Such processes account for a small portion (2%) of the growing

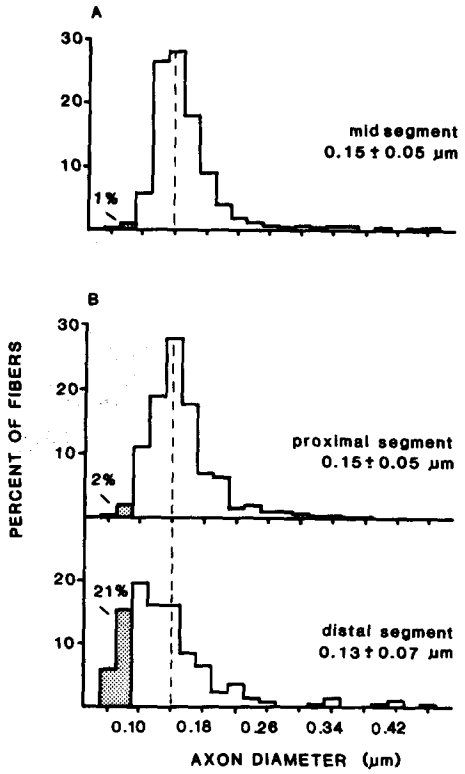

FIGURE 4 Frequency histogram of diameters of axon shafts from mature and growing (5-wk-postoperative) olfactory nerves of the bullfrog. (*A*) The average diameter of axons in mature nerves, 0.15 ± 0.05 μm ($\bar{X}$ ± SD, n = 668), is the same when calculated from thin-sectioned or freeze-fractured preparations. The distribution shows a positive skew toward larger fiber diameters. No regional differences in axon diameter were observed in different segments of mature nerve. (*B*) In growing nerves, the size histogram of diameters of axon shafts shifts to the left, toward smaller diameters, in more distal portions of the nerve. Average fiber diameter decreases significantly from 0.15 ± 0.05 μm (n = 377) proximally to 0.13 ± 0.07 μm (n = 223) distally. The growing fiber population shows greater variability in size than seen in mature axons. Growth cones are excluded from this sample because their profiles are too irregular in shape to be measured with the procedure used for shafts.

fiber population intranasally, but increase to 21% of the population distally (cf. 5). Throughout the mature nerve, however, they are rarely seen (1%).

Membranes of Mature Olfactory Neurons

When segments of mature olfactory nerve are longitudinally fractured, vast numbers of axonal P- and E-faces are exposed for various distances in the replicas (Fig. 2*B*); P-faces appear as convex and E-faces appear as concave leaflets. The structure of fractured P-face membranes from mature olfactory perikarya and axons is shown in Fig. 5, *A* and *B*. The calculated densities of axonal P-face IMPs of all sizes are shown, for several segments of mature nerve, in Fig. 7 and in Table I. The most proximal nerve segment sampled was from the submucosa, where the axons have already formed large fiber bundles (cf. below). The most distal region of the nerve analyzed was the olfactory nerve layer within the olfactory bulb; synaptic terminals in glomeruli of the bulb are not included in this study. When IMP density data from proximal, middle, and distal regions of the nerve are compared, no significant differences in total P- or E-face densities are found along the shafts of mature axons (Table I). The combined P-face axonal density for all nerve segments is 907 ± 24 IMPs/μm^2; overall E-face density is 487 ± 23 IMPs/μm^2.

Perikaryal plasmalemma of the mature olfactory neuron shows a distinctly different density of IMPs. Perikaryal P-face IMP density (2,756/μm^2) is three times as high as that observed along the axonal shaft (907/μm^2; $P < 0.001$). The transitional zone bridging perikaryal and axonal membrane, the axon hillock, was identified in two cases. The IMP density of a 0.3 μm length of the axon hillock was similar to that of the perikaryal plasma membrane (~2,700/μm^2). The nearest distal region of neuritic plasma membrane that we were able to sample was submucosal, and thus ~150 μm away from the axon hillock. This suggests that, somewhere between the axon hillock and the submucosa, a sharp decrease in particle density occurs.

IMP-size histograms were generated for identified nerve segments. Axonal IMP size-classes range from ~3 to 14.8 nm. Because their appearance is so dependent on the relative angle of shadowing and replica grain size, the smallest particles were combined in a ≤4.0-nm class. Axolemma from the most proximal and distal segments of the mature nerve contains similar profiles of the differently sized particles as seen in Fig. 8*A*. The most frequent IMP observed along the mature axon is a 6.7-nm particle. IMPs ≥8.1 nm account for 27% of the total P-face particles in both proximal and distal regions of mature axons. The IMP size histogram of perikaryal plasmalemma is also shown in Fig. 8*A*. Relative densities of each IMP size class are somewhat similar to those of axolemma,

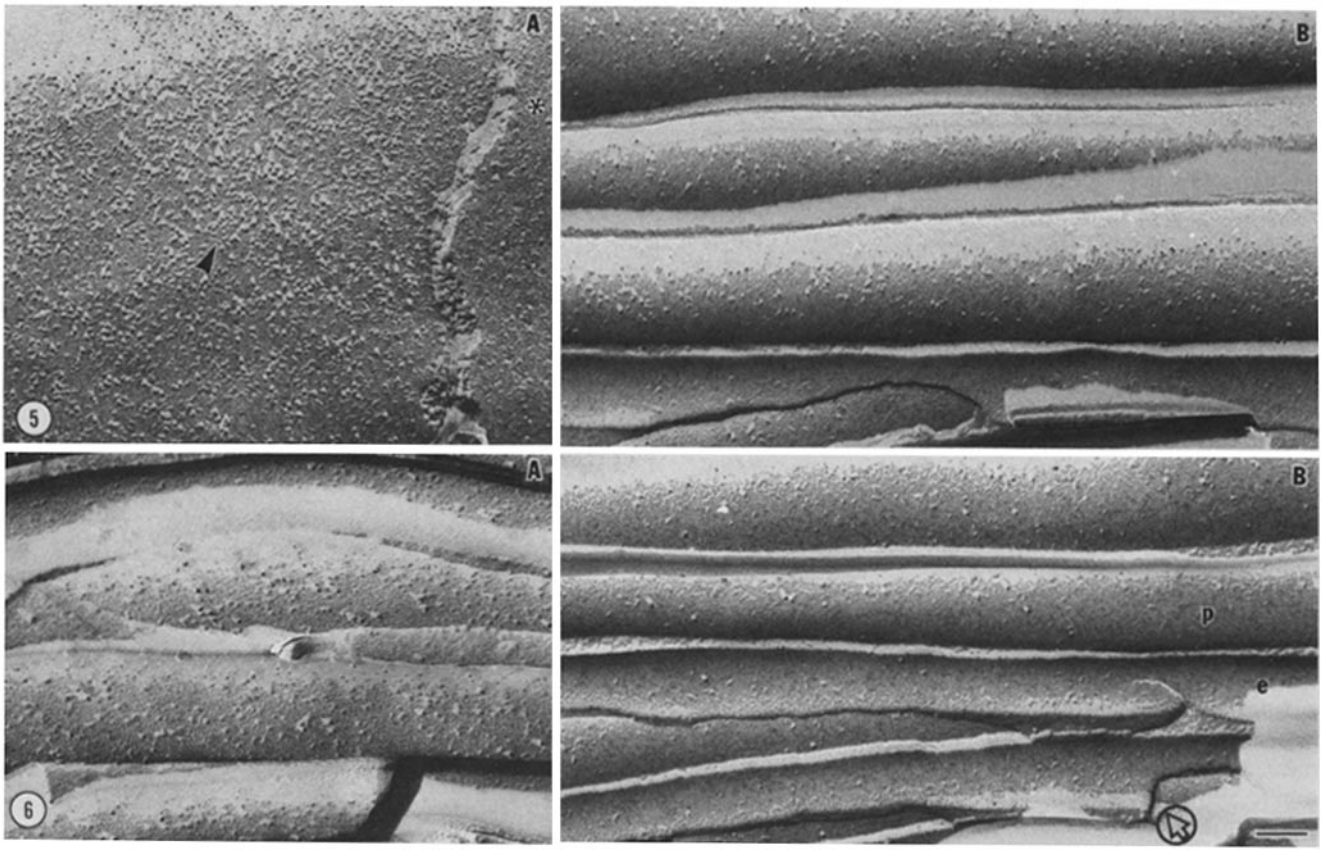

FIGURES 5 and 6 Freeze-fractured plasma membrane of olfactory neurons at different stages of maturity. Fig. 5: (*A*) Perikaryon of mature olfactory neuron at the level of the nucleus shows a P-face IMP density that is three times as high as that of the axon. Arrowhead indicates an example of an oblong particle. Asterisk indicates the E-face of an adjacent unidentified cell. (*B*) Mature olfactory axons from a mid segment of the nerve for comparison (convex profiles are P-faces, concave profiles are E-faces). Fig. 6: (*A*) Growing olfactory axons (5-wk-postoperative) from a proximal nerve segment show high P- and E-face IMP densities. (*B*) Growing olfactory axons (5-wk-postoperative) from a distal nerve segment. Note low P- and E-face IMP densities (*p* and *e*, respectively) compared to more proximal or mature axons. Circled arrow indicates approximate shadowing direction. Bar, 0.1 μm. × 71,000.

TABLE I

Comparison of the Mean IMP Density in Plasma Membranes of Mature and Growing Olfactory Neurons

	P-face				E-face			
	Density	No. of axons/ cells	Total area	No. of replicas	Density	No. of axons/ cells	Total area	No. of replicas
	IMPs/μm²		*μm²*		*IMPs/μm²*		*μm²*	
Mature olfactory neurons								
Perikarya	2,756 ± 124	6	2.4	4				
Axons: Overall	907 ± 24*	116	19.7	12	487 ± 23	54	7.3	11
Segments‡								
0.00–0.33	898 ± 50	25	4.0	4	543 ± 48	11	2.1	3
0.34–0.66	869 ± 44	46	8.1	4	492 ± 38	24	3.6	4
0.67–1.00	946 ± 30	45	7.6	4	476 ± 32	17	1.6	4
Growing olfactory neurons								
Perikarya	2,591 ± 261	5	2.3	4				
Axons:								
Segments‡								
0.00–0.33	1,082 ± 35	60	5.3	4	624 ± 43	15	1.7	2
0.34–0.66	690 ± 13*	325	46.3	7	425 ± 25*	31	3.1	5
0.67–1.00	478 ± 12*	336	60.0	6	308 ± 23*	54	7.0	3

* Significant difference ($P < 0.001$) between this number and the one directly above.
‡ Distance from the perikaryon as fraction of total length. All values are $\bar{x} \pm$ SEM.

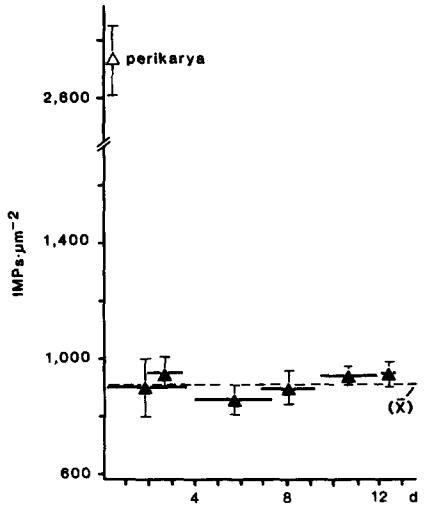

FIGURE 7 IMP densities (P-face) in the plasmalemma of mature olfactory neurons, plotted as a function of the distance from the perikaryon. The overall density of all regions (excluding the perikaryon and axon hillock) is indicated as a dashed line ($\bar{X}$). The distance of each replicated nerve segment from the origin, *d*, has been normalized on the basis of the calculated average length of mature nerves (cf. Materials and Methods). Perikaryal densities are approximately three times higher than those of mature axonal shafts. Note that the most proximal IMP densities sampled were from the submucosa which is ~150 μm distant from the beginning of the axon hillock.

but absolute densities are much higher. As in the axon, the most common IMP in the perikarya is a 6.7-nm particle. In addition, the perikaryon contains low densities of large IMPs (>14.8 nm) that are not present in the axon.

Schwann cell plasma membrane is easily distinguished from axolemma in replicas of the nerve on the basis of its configuration and location at the periphery of axon bundles. The Schwann cell's P-face IMP density of 2,218 ± 58/μm² and E-face density of 1,957 ± 136/μm² are considerably higher than the respective values of axons.

Membranes of Growing Olfactory Neurons (5 wk after Surgery)

AXONS: Freeze-fracture images of immature nerve at early stages of growth are consistent with the observations made in thin sections: only small numbers of axons are bundled together, and the fascicles are widely separated by extracellular space (Fig. 3, *A* and *B*). At higher power, the morphologic appearance of axolemma (Fig. 6, *A* and *B*) indicates the presence of different IMP densities in proximal and distal regions of growing nerve. A comparison of IMP densities along the somatofugal axis reveals a significant ($P < 0.001$) decrease in the average P-face densities from 1,082/μm² in the proximal region, to 690/μm² (middle region), to 478/μm² in the distal region (Table I). E-face IMP densities also decrease significantly along the somatofugal axis by a factor of about 0.5 times. The densities of P-face IMPs from segments of growing nerve are plotted in Fig. 9 as a function of distance from the perikaryon. Data from eight nerves are included in this figure. The total density of IMPs on axonal shafts forms a strongly decreasing gradient along the somatofugal axis, from ~1,100 IMPs/μm² near the perikarya to ~350 IMPs/μm² at the distal ends. The data points are well fitted by the decreasing exponential function, $y = 1{,}442e^{-0.15x}$ ($r^2 = 0.92$) shown in Fig. 9.

IMP-size histograms for axolemma of proximal and distal segments of growing nerve (5-wk-postoperative) are shown in Fig. 8*B*. A striking difference in the shape of the two profiles can be observed, suggesting a relative difference in populations of membrane components. Table II shows the ratio (for each IMP-size class) of particle density in the proximal axolemma to particle density in the distal axolemma. It is clear that the quasi exponential gradient describing total densities (Fig. 9) does not result from equal reduction in all IMP size classes. Instead, the extent of the reduction increases with particle diameter so that the largest IMPs show the greatest fractional reduction. IMPs ≥8.1-nm diameter account for 25% of the IMP population proximally, but only 11% of the population distally; these large IMPs are from 4 to 16 times more frequent

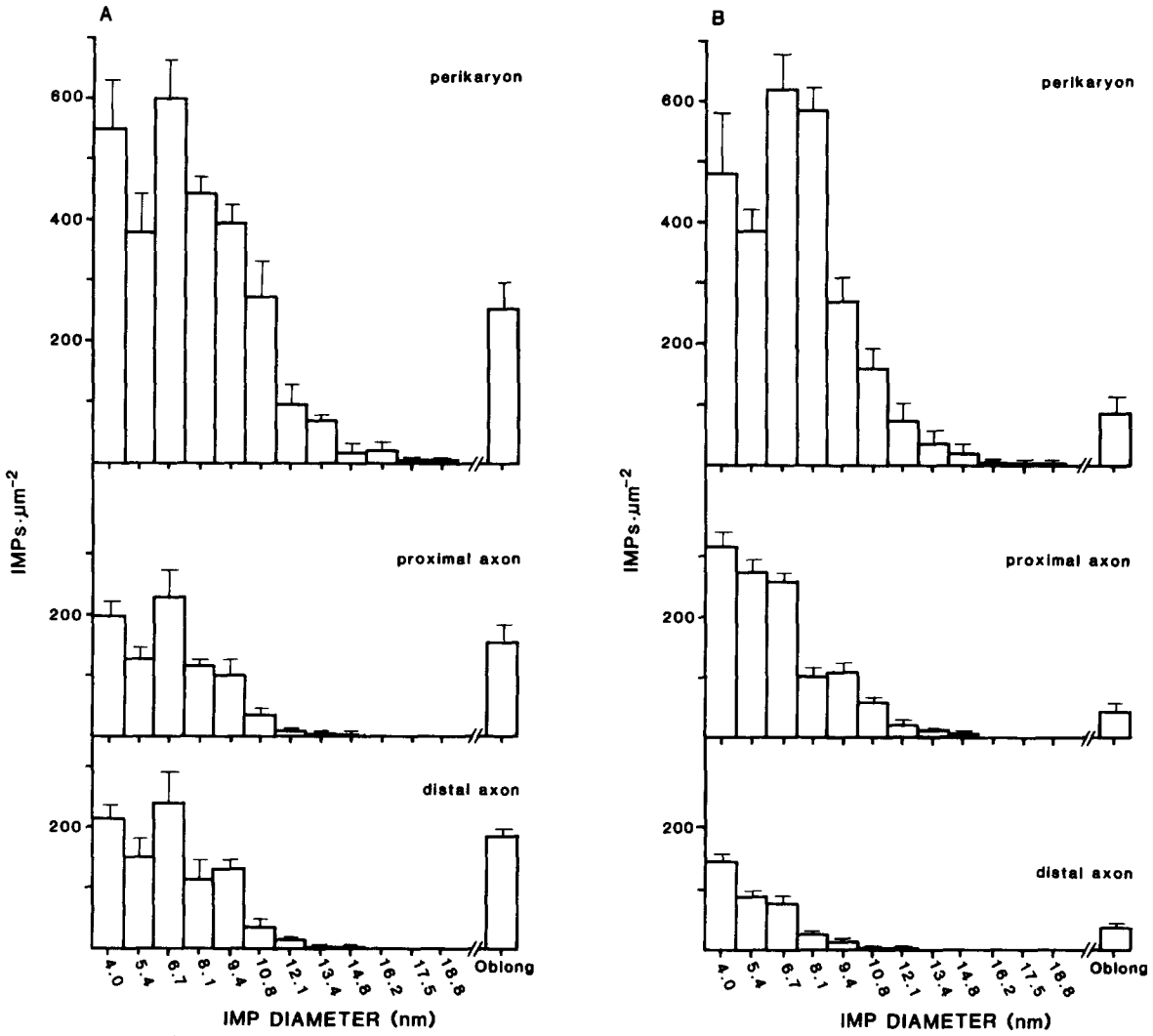

FIGURE 8 IMP size histograms from three different regions of mature (*A*) and growing (*B*) olfactory neurons. P-face densities ($\bar{X}$ ± SEM) of each IMP size class and oblong particles are indicated. (*A*) In mature neurons, perikaryal IMP density is considerably higher (three times) than the axonal density, but the relative frequencies of differently sized IMPs are similar. Proximal and distal portions of the axon also have similar IMP profiles. (*B*) The growing neuron (5-wk-postoperative) shows different IMP profiles in the perikaryon and proximal and distal axons. The relative reduction in density of each IMP size class, in the distal compared to the proximal axon, increases with particle diameter (cf. Table II). The smallest particles were combined in a ≤4.0-nm class for reasons described in the text.

in proximal than in the distal regions of growing axons (Table II).

The density of individual IMP size classes was analyzed as a function of the distance from the perikaryon. Data from three representative classes, 6.7, 9.4, and 10.8 nm, and their curves of best fit are shown in Fig. 10*A*. The distribution of each IMP-size class along the neuritic axis forms a distally decreasing, approximately exponential function. Furthermore, Fig. 10*A* suggests that the density gradients for individual IMP-size classes differ in shape. As shown in Fig. 10*B*, density gradients form a family of decreasing, quasi exponential functions whose slopes increase with particle diameter (cf. *b* in Table III). This is true for all but the 13.4-nm IMPs, whose counts were very small.

GROWTH CONES: Growth cones in vivo appear in fractures as irregularly shaped enlargements at the tip of a thin, tubular process (Fig. 11). The growth cone often contains one or more endo- or exocytotic figures near its base and, when cross-fractured as in Fig. 11*A*, vesicle clusters are apparent. Long filopodia are not easily identified in these preparations.

Because the pattern of plasmalemmal IMPs on the growth cone (Fig. 11) differs from that of the distal axonal shaft (Fig. 6*B*), growth cone particle density was analyzed separately. Limited regions of P-face membrane located at the base of the growth cone, near the axonal shaft, and more peripheral discrete zones contain relatively high IMP densities of 827 ± 120 IMPs/μm^2. Between these high-density zones, the growth cone is almost free of IMPs, showing only 185 ± 19 IMPs/μm^2. These measurements were obtained by counting particles in membrane areas well enclosed within these two domains. The result is a mosaic pattern of particle densities or microheterogeneity of the growth cone plasmalemma. Such regional shifts in IMP density are not seen in the axonal shafts.

Separate size histograms were calculated for the two regions of the growth cone previously distinguished on the basis of

IMP density. Although the total particle counts are very different for the two regions, the shapes of the IMP size histograms for high-density domains (Fig. 12*A*) and low-density domains (Fig. 12*B*) suggest that they share a qualitatively similar particle composition. The extent of this similarity is even more obvious in Fig. 12*C*, which compares the relative densities of each size particle for high- and low-density domains. Fig. 12*C* also includes the relative IMP size distribution for distal shaft axolemma to better illustrate the difference between the axonal and the growth cone particle populations. While growth cone plasmalemma contains lower densities of the small IMP size classes, it is relatively rich in large IMPs (≥8.1 nm) when compared to the distal shaft (cf. open arrowheads, Fig. 11*D*). Large particles account for ~39% of the total growth cone IMP population in high-density regions and 32% in low-density regions, but only 11% in the distal axolemma. The IMP profiles clearly indicate a distinction in the components of the axonal and the growth cone plasma membranes.

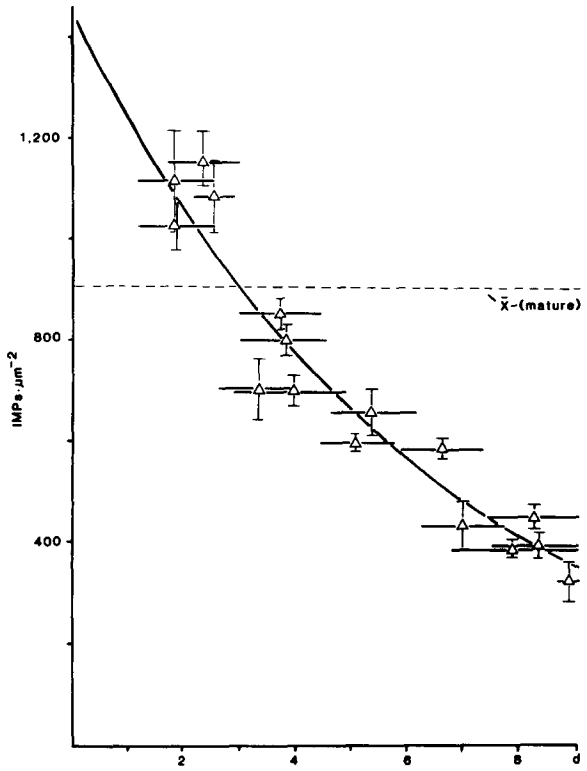

FIGURE 9 Particle density (P-face) of the growing axon (5-wk-postoperative) decreases exponentially in somatofugal direction. Average densities ± SEM, from individual replicas of segments taken from eight nerves are included. The horizontal bars indicate the lengths of the segments for the respective density values. The data is well fitted by the exponential function, $y = 1{,}442e^{-0.15x}$ (r^2 = 0.92), indicated in the figure.

VESICLES: Clusters of clear vesicles are characteristically found in sprouting neurites, especially at growth cones (4, 39, 43). Vesicles are usually spherical in shape, averaging 80 nm

TABLE II

Ratio of P-face IMP Densities in the Proximal and Distal Segments of Mature and Growing Olfactory Axons

	Proximal IMPs/μm²/Distal IMPs/μm²	
IMP diameter	Mature axons	Growing axons (5 wk)
nm		
≤4.0	0.93	2.16
5.4	0.83	3.13
6.7	0.95	3.39
8.1	1.04	4.00
9.4	0.75	8.49
10.8	1.00	12.93
12.1	0.65	18.06
13.4	1.00	15.81
14.8	1.00	—

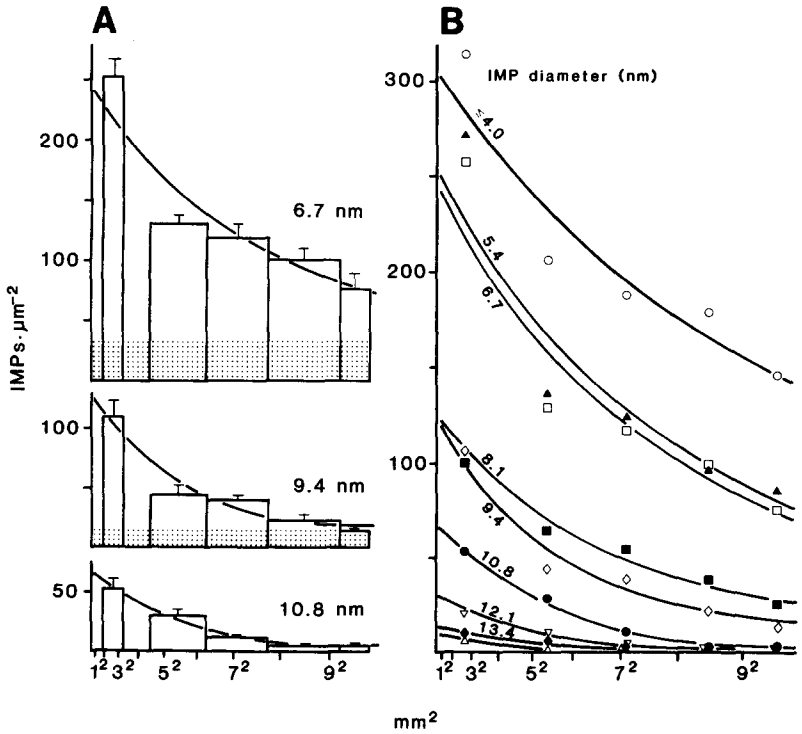

FIGURE 10 When P-face densities of individual IMP size classes are calculated in the growing (5-wk-postoperative) nerve, each IMP size class shows a decreasing density gradient which is well fitted by an exponential function (cf. Table III). Examples of such IMP density profiles are plotted in *A* for 6.7-, 9.4-, and 10.8-nm particles, and the functions of best fit are shown. The abscissa represents the squared distance from the perikarya. This distance, in millimeters, has been normalized on the basis of the average length of 5-wk growing nerves. Stiple indicates the density of particles contained in the clear vesicles that occur clustered in growth cones and are the putative source of newly inserted axolemma. (*B*) Density gradients and exponential functions of best fit of all particle size classes. Note that the slope of each gradient increases with particle diameter for all but the 13.4-nm particles (cf. Table III for formulas and r^2 values of the gradients). These exponential functions are Gaussian and, therefore, suggest diffusion kinetics of the IMPs within the axolemma (36). The largest IMP size (upright open triangle) is 14.8 nm.

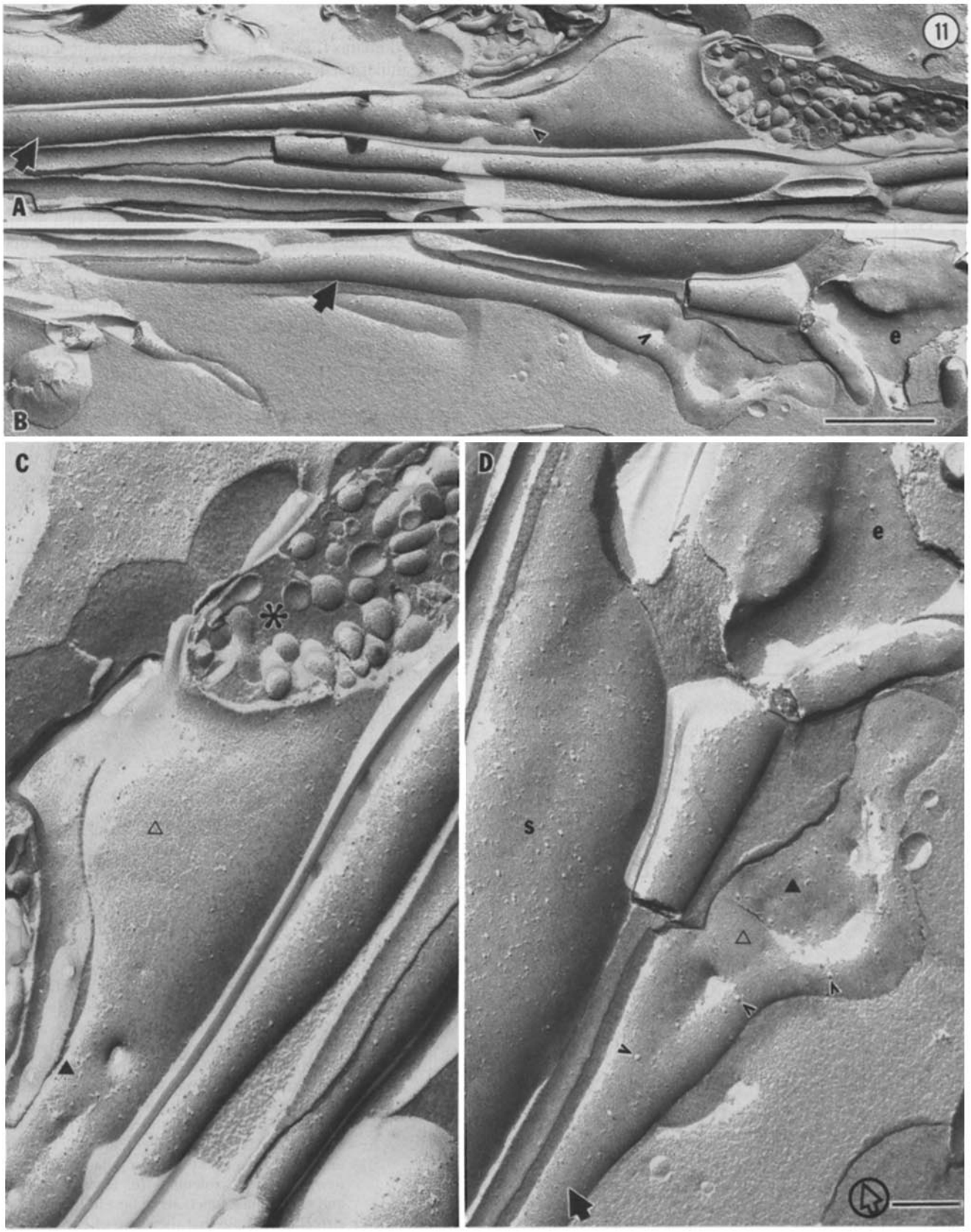

FIGURE 11 Growth cones from growing olfactory nerves (5-wk-postoperative) display a unique IMP profile that differs from that of axonal shafts. (*A* and *B*) Fractured growth cones in vivo are recognized as enlarged endings on thin tubular processes. The morphology of the growth cone varies but frequently includes one or more endo- or exocytotic profiles (open arrowheads). Even at low magnification, a regional shift in IMP density from the axonal shaft (arrows) to the growth cone is apparent. Bar, 0.5 μm. × 40,000. (*C* and *D*) The growth cone displays a mosaic pattern or microheterogeneity of particle densities; limited regions such as the base of the growth cone in C show a high IMP density (solid triangles) while adjacent regions are particle-poor (open triangle). Asterisk indicates a vesicle cluster that is characteristic of growth cones. These vesicles contain a sparse population of small particles (P-face density 175 IMPs/μm^2). (*D*) The IMP size profile of growth cones is richer in large IMPs (open arrowheads) than the adjacent axonal shaft (arrow). The plasma membrane abruptly shifts from domains of high (solid triangle) to low (open triangle) particle density. An adjacent growth cone E-face (e) and Schwann cell (s) are indicated. Bar, 0.2 μm. × 75,000. Circled arrow indicates approximate shadowing direction.

TABLE III

Exponential Functions of Best Fit for Density Gradients of Individual IMP-size Classes in Growing Olfactory Nerves (5-wk-postoperative)

IMP diameter	$y = ae^{-bx^2} + c$			
	a	b	c*	r^2
nm				
≤4.0	304	0.0127	74	0.90
5.4	251	0.0166	32	0.91
6.7	244	0.0180	35	0.91
8.1	124	0.0230	14	0.94
9.4	124	0.0352	14	0.95
10.8	68	0.0356	—	0.90
12.1	30	0.0357	—	1.00
13.4	14	0.0314	—	0.94
14.8	10	0.0544	—	0.93

* Density of IMPs in vesicles characteristic of growth cones (see Materials and Methods).

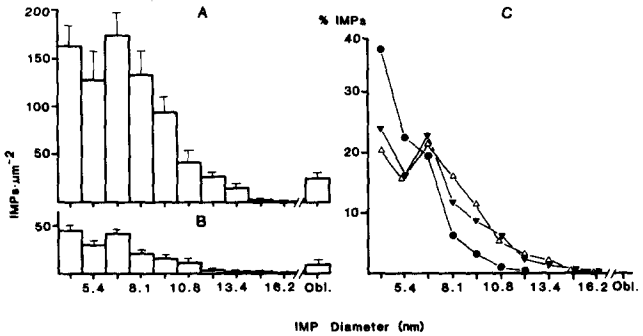

FIGURE 12 Growth cones display a mosaic pattern of high and low IMP density domains. (*A*) High-density regions have an average P-face density of 827 ± 19 IMPs/μm^2, and they are qualitatively similar (size histograms) to low-density regions (*B*), which have an average P-face density of only 185 ± 19 IMPs/μm^2. In *C*, comparison of the relative profiles of high-density (△) and low-density (▼) regions of growth cones shows more clearly that these exhibit very similar particle populations, which are relatively rich in large IMPs. However, they are quite different from those of the distal axonal shafts (●), which are poor in large IMPs. Particle profiles were normalized by expressing the density of each size class as a percentage of the total IMP population.

TABLE IV

Comparison of P-face IMP Densities in Growth Cones, Vesicles, and Distal Shafts

IMP diameter	Growth cones (low-density zones)	Vesicles	Distal shafts
nm	μm^{-2}	μm^{-2}	μm^{-2}
≤4.0	45	74	146
5.4	30	32	87
6.7	42	35	76
8.1	22	14	25
9.4	16	14	13
10.8	12	—	4
12.1	4	—	1
13.4	3	—	1
14.8	1	—	—

in diameter, and are believed to be the plasmalemmal precursor (26, 32). IMP analysis of the concave P-face reveals a sparse population of primarily small IMPs (Table IV). This population is more similar to the IMPs found in the plasmalemma of the distal axon shaft than to those in the growth cone, which is relatively enriched in large particles (cf. Fig. 12).

DISCUSSION

The biochemical nature of IMPs is not fully understood (cf. below), but it is highly likely that the appearance of their constituents is influenced in some way by fixation, freezing, fracturing, and replicating procedures. Nevertheless, IMP size and frequency are valuable parameters for comparing membrane types and regions so long as the processing conditions were consistent throughout experimentation.

Axolemmal Structure of Growing and Mature Nerves

Comparison of intramembrane structure of mature and growing axolemma reveals major differences. While the particle population in plasmalemma of the mature axon's shaft is essentially uniform, both qualitatively and quantitatively, there is a major reduction in particle density along the growing axon as one moves in a somatofugal direction. These data are consistent with those obtained earlier by Pfenninger and Bunge (29) and by Garcia-Segura and Perrelet (7). However, the favorable properties of the olfactory nerve system have enabled us to investigate the distal reduction of IMPs in far greater detail: Not only does the overall number of particles decrease, but the ratios of IMPs in proximal vs. distal axolemma rise from 2.2 to 18.1 with increasing particle size. The analysis of the density of each IMP-size class as a function of the distance from the perikaryon reveals a pattern of continuously changing particle populations in proximodistal direction in the growing nerve. These gradual changes are generated by the distribution functions of the IMP-size classes, which are approximately exponential in nature and whose slopes are a function of particle size (cf. 36).

Perikarya as well as growth cones are excluded from this complex set of exponential gradients in the growing nerve. In both the mature and the growing neuron, there is a sharp decrease in the density of IMPs from the perikaryon to the proximal axonal shaft. The axolemma of the most proximal growing shaft, however, is somewhat richer in IMPs than that of its mature counterpart, primarily due to an increase in small IMPs. The other extreme end of the axon also contains a somewhat sudden shift in plasmalemmal IMP composition: Although axonal endings of the mature olfactory nerve have not been included in this study, the presynaptic membrane has long been known to be the site of accumulation of particles of various sizes, especially large ones (e.g., 14, 24, 28). Growth cone plasmalemma, whose mean IMP density is about as low as that of the distal shaft, was found to be heterogeneous, comprising domains of relatively high IMP density and areas with very low particle counts. In both of these growth cone regions, however, the particle populations are quite different from that of the distal shaft, showing a relative enrichment in large particles.

Specific Membrane Composition of the Growing Axon

This study presents detailed ultrastructural data that distinguish axonal shaft and growth cone from other parts of the growing neuron and from any membrane region in the ma-

ture, synapsing neuron. Strong evidence, mainly from reconstitution experiments (e.g., 15, 19, 34, 35) supports the widely held view that at least some IMPs represent complexes of integral membrane proteins. Yet, it is not clear (*a*) whether all classes of such proteins form particles, (*b*) whether some of them have to aggregate to be seen, or (*c*) whether lipids participate in IMP formation or can, by themselves, form IMPs (for reviews, see, for example, references 20, 33, 40). Nevertheless, our observations indicate that growth cone plasmalemma and axolemma of the growing neurite are biochemically as well as functionally distinct—as one would expect from the special functional needs of these structures. This conclusion is consistent with the recent lectin labeling data of Pfenninger and Maylié-Pfenninger (31), which have demonstrated that plasmalemmal glycoconjugate composition changes in the form of gradients as one moves from the perikaryon to the growth cone. The discovery of regional differences in the frequency of large IMPs raises the question of differences in the density of ion channels as examples of transmembrane proteins. As reported in one of the companion papers (38), regional differences in sodium channel density exist in the growing axon. Furthermore, electrophysiological data suggest the prevalence of voltage-dependent calcium channels at the growing tip of neurites (12, 17, 21).

Particle Density Gradients and Their Relationship to the Mechanism of Axolemmal Expansion

IMP density gradients can be observed in axons only as long as these are in the process of elongation. A steadily increasing body of evidence indicates that plasmalemmal expansion necessary for axonal growth is achieved by distal insertion of new components (2, 3, 30, 32), probably as preformed membrane vesicles. Although it has been argued that "growth cone vesicles" are a fixation artifact (13; but see reference 25), radioautographic evidence suggests that they are the plasmalemmal precursor (26, 27). If the vesicles are indeed the plasmalemmal precursor, as we propose, the newly inserted membrane should be poor in IMPs, particularly the large ones. This is actually the case (cf. Table IV). On the other hand, the IMP density gradients found in the growing axon indicate a gradual appearance in its plasmalemma of specific membrane components brought from the perikaryon—a proximodistal maturation process of the young axolemma. The approximately exponential nature and the size-dependence of IMP gradients (large particles arrive in a specific axolemmal segment at a slower rate than the smaller ones) strongly suggest that IMPs reach distal axolemma by diffusion within the axolemma itself. Given the rapid rate of axonal elongation (0.35 mm/d) and the considerable length of olfactory axons, IMP diffusion may not reach equilibrium until after axonal elongation has stopped for synaptogenesis. IMP diffusion gradients in the plasmalemma, as evaluated by mathematical analysis, are the subject of one of the companion papers (36). Our current hypothesis views the IMP density gradients as a result of insertion of the respective membrane components into perikaryal plasmalemma, followed by proximodistal diffusion into growing axolemma. This would be a maturation process that follows insertion of a specific, particle-poor membrane at the growth cone.

The authors thank Dr. Martin Blank for his advice regarding the mathematical analysis of the particle gradients, Linda B. Friedman for excellent technical assistance and Kathleen Silberman for expert secretarial help with the completion of this manuscript.

The research was supported by National Institutes of Health grant NS13466 to K. H. Pfenninger and New York State Health Research Council grant 164842 to R. Small. Dr. Small was also a Jordan fellow of the National Spinal Cord Injury Foundation.

Received for publication 21 September 1982, and in revised form 30 September 1983.

REFERENCES

1. Besharse, J. C., and K. H. Pfenninger. 1980. Membrane assembly in retinal photoreceptors. I. Freeze-fracture analysis of cytoplasmic vesicles in relationship to disc assembly. *J. Cell Biol.* 87:451–463.
2. Bray, D. 1970. Surface movements during the growth of single explanted neurons. *Proc. Natl. Acad. Sci. USA* 65:905–910.
3. Bray, D. 1973. Branching patterns of isolated sympathetic neurons. *J. Cell Biol.* 56:702–712.
4. Bunge, M. B. 1973. Fine structure of nerve fibers and growth cones of isolated sympathetic neurons in culture. *J. Cell Biol.* 56:713–735.
5. Cancalon, P., and J. S. Elam. 1980. Study of regeneration in the garfish olfactory nerve. *J. Cell Biol.* 84:779–794.
6. Easton, D. M. 1971. Garfish olfactory nerve: easily accessible source of numerous long, homogeneous, nonmyelinated axons. *Science (Wash. DC).* 172:952–955.
7. Garcia-Segura, L. M., and A. Perrelet. 1981. Freeze-fracture of developing neuronal plasma membrane in postnatal cerebellum. *Brain Res.* 208:19–33.
8. Gasser, H. S. 1956. Olfactory nerve fibers. *J. Gen. Physiol.* 39:473–496.
9. Graziadei, P. P. C. 1973. Cell dynamics in the olfactory mucosa. *Tissue Cell.* 5:113–131.
10. Graziadei, P. P. C., and R. S. DeHan. 1973. Neuronal regeneration in frog olfactory system. *J. Cell Biol.* 59:525–530.
11. Grefrath, S. P., and J. A. Reynolds. 1973. Polypeptide components of an excitable plasma membrane. *J. Biol. Chem.* 248:6091–6094.
12. Grinvald, A., and I. C. Farber. 1981. Optical recording of calcium action potentials from growth cones of cultured neurons with a laser microbeam. *Science (Wash. DC).* 212:1164–1167.
13. Hasty, D. L., and E. D. Hay. 1978. Freeze fracture studies of the developing cell surface. II. Particle-free membrane blisters on glutaraldehyde-fixed corneal fibroblasts are artifacts. *J. Cell Biol.* 78:756–768.
14. Heuser, J. E., T. S. Reese, and D. M. D. Landis. 1974. Functional changes in frog neuromuscular junctions studied with freeze fracture. *J. Neurocytol.* 3:109–131.
15. Hong, K., and W. L. Hubbell. 1972. Preparation and properties of phospholipid bilayers containing rhodopsin. *Proc. Natl. Acad. Sci. USA* 69:2617–2621.
16. Kreutzberg, G. W., and G. W. Gross. 1977. General morphology and axonal ultrastructure of the olfactory nerve of the pike, *Esox lucius. Cell Tissue Res.* 181:443–457.
17. Llinas, R., and M. Sugimori. 1979. Calcium conductances in Purkinje cell dendrites: their role in development and integration. *In* Development and Chemical Specificity of Neurons, Progress in Brain Research. M. Cuénod, G. W. Kreutzberg, and F. E. Bloom, editors. Elsevier/North Holland Biomedical Press, Amsterdam. 51:323–334.
18. Losa, G. A., E. R. Weibel, and R. P. Bolender. 1978. Integrated stereological and biochemical studies on hepatocytic membranes. *J. Cell Biol.* 78:289–308.
19. McLennon, D. H., P. Seeman, G. H. Isles, and C. C. Yip. 1971. Membrane formation by the adenosine triphosphatase of sarcoplasmic reticulum. *J. Biol. Chem.* 246:2702–2710.
20. McNutt, N. S. 1977. Freeze-fracture techniques and applications to the structural analysis of the mammalian plasma membrane. *Cell Surf. Rev.* 3:95–126.
21. Meiri, H., M. E. Spira, and I. Parnas. 1981. Membrane conductances and action potential of a regenerating axonal tip. *Science (Wash. DC).* 211:709–712.
22. Morré, D. J., J. Kartenbeck, and W. W. Franke. 1979. Membrane flow and interconversions among endomembranes. *Biochim. Biophys. Acta.* 559:71–152.
23. Palade, G. E. 1975. Intracellular aspects of the process of protein secretion. *Science (Wash. DC).* 189:347–358.
24. Peper, K., F. Dreyer, C. Sandri, K. Akert, and H. Moor. 1974. Structure and ultrastructure of the frog motor endplate: a freeze-etching study. *Cell Tissue Res.* 149:437–455.
25. Pfenninger, K. H. 1979. Subplasmalemmal vesicle clusters: real or artifact? *In* Freeze-Fracture: Methods, Artifacts, and Interpretations. J. E. Rash and C. S. Hudson, editors. Raven Press, New York. pp. 71–80.
26. Pfenninger, K. H. 1980. Mechanism of membrane expansion in the growing neuron. *Soc. Neurosci. Abstr.* 6:661.
27. Pfenninger, K. H. 1982. Axonal transport in the sprouting neuron: transfer of newly synthesized membrane components to the cell surface. *In* Axoplasmic Transport in Physiology and Pathology. D. G. Weiss and A. Gorio, editors. Springer Verlag/Berlin, Heidelberg. pp. 52–61.
28. Pfenninger, K., K. Akert, H. Moor, and C. Sandri. 1972. The fine structure of freeze-fractured presynaptic membranes. *J. Neurocytol.* 1:129–149.
29. Pfenninger, K. H., and R. P. Bunge. 1974. Freeze-fracturing of nerve growth cones and young fibers: a study of developing plasma membrane. *J. Cell Biol.* 63:180–196.
30. Pfenninger, K. H., and M. P. Johnson. 1983. Membrane biogenesis in the sprouting neuron. I. Selective transfer of newly synthesized phospholipid into the growing neurite. *J. Cell Biol.* 97:1038–1042.
31. Pfenninger, K. H., and M.-F. Maylié-Pffeninger. 1981. Lectin labeling of sprouting neurons. I. Regional distribution of surface glycoconjugates. *J. Cell Biol.* 89:536–546.
32. Pfenninger, K. H., and M.-F. Maylié-Pfenninger. 1981. Lectin labeling of sprouting neurons. II. Relative movement and appearance of glycoconjugates during plasmalemmal expansion. *J. Cell Biol.* 89:547–559.
33. Satir, B, and P. Satir. 1979. Partitioning of intramembrane particles during the freeze-fracture procedure. *In* Freeze-Fracture: Methods, Artifacts, and Interpretations. J. E. Rash and C. S. Hudson, editors. Raven Press/New York. pp. 43–49.
34. Segrest, J. P., T. Gulik-Krzywicki, and C. Sardet. 1974. Association of the membrane-penetrating polypeptide segment of the human erythrocyte MN-glycoprotein with phospholipid bilayers. I. Formation of freeze-etch intramembranous particles. *Proc. Natl. Acad. Sci. USA* 71:3294–3298.
35. Skriver, E., A. B. Maunsbach, and P. L. Jorgensen. 1980. Ultrastructure of Na,K-transport vesicles reconstituted with purified renal Na,K-ATPase. *J. Cell Biol.* 86:746–754.

36. Small, R. K., M. Blank, R. Ghez, and K. H. Pfenninger. 1983. Components of the plasma membrane of growing axons. II. Diffusion of membrane protein complexes. *J. Cell Biol.* 98:1434–1443.
37. Strichartz, G., R. Small, C. Nicholson, K. Pfenninger, and R. Llinas. 1980. Ionic mechanisms for impulse propagation in growing nonmyelinated axons: saxitoxin binding and electrophysiology. *Soc. Neurosci. Abstr.* 6:660.
38. Strichartz, G. R., R. K. Small, and K. H. Pfenninger. 1983. Components of the plasma membrane of growing axons. III. Saxitoxin binding to sodium channels. *J. Cell Biol.* 98:1444–1452.
39. Tennyson, V. M. 1970. The fine structure of the axon and growth cone of the dorsal root neuroblast of the rabbit embryo. *J. Cell Biol.* 44:62–79.
40. Verkleij, A. J., and P. H. J. T. Ververgaert. 1978. Freeze-fracture morphology of biological membranes. *Biochem. Biophys. Acta.* 515:303–327.
41. von Muralt, A., E. R. Weibel, and J. V. Howarth. 1976. The optical spike: structure of the olfactory nerve of pike and rapid birefringence changes during excitation. *Pflügers Archiv.* 367:67–76.
42. Wald, F. 1972. Ionic differences between somatic and axonal action potentials in snail giant neurones. *J. Physiol. (Lond.).* 220:267–281.
43. Yamada, K. M., B. S. Spooner, and N. K. Wessels. 1971. Ultrastructure and function of growth cones and axons of cultured nerve cells. *J. Cell Biol.* 49:614–635.